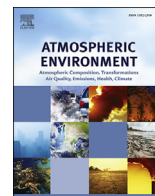


Contents lists available at [ScienceDirect](http://www.sciencedirect.com)

Atmospheric Environment

journal homepage: www.elsevier.com/locate/atmosenv

The relationships between insoluble precipitation residues, clouds, and precipitation over California's southern Sierra Nevada during winter storms



Jessie M. Creamean^{a, b, *}, Allen B. White^b, Patrick Minnis^c, Rabindra Palikonda^d,
Douglas A. Spangenberg^d, Kimberly A. Prather^{e, f}

^a Cooperative Institute for Research in Environmental Sciences, University of Colorado, Boulder, CO, USA

^b NOAA Earth System Research Laboratory, Physical Sciences Division, Boulder, CO, USA

^c NASA Langley Research Center, Hampton, VA, USA

^d Science Systems and Applications, Inc., Hampton, VA, USA

^e Department of Chemistry and Biochemistry, University of California at San Diego, La Jolla, CA, USA

^f Scripps Institution of Oceanography, University of California at San Diego, La Jolla, CA, USA

HIGHLIGHTS

- Dust and biological residue particles likely INPs found in Yosemite snow.
- Dust more prevalent at higher elevations due to long-range transport.
- Ice clouds present during prevalence of biological and calcium dust residues.
- Dust and biological residues correlated with higher precipitation quantities.

ARTICLE INFO

Article history:

Received 10 February 2016

Received in revised form

31 May 2016

Accepted 6 June 2016

Available online 8 June 2016

Keywords:

Aerosol-cloud-precipitation interactions

Ice nucleation

Cloud glaciation

Sierra nevada

ABSTRACT

Ice formation in orographic mixed-phase clouds can enhance precipitation and depends on the type of aerosols that serve as ice nucleating particles (INPs). The resulting precipitation from these clouds is a viable source of water, especially for regions such as the California Sierra Nevada. Thus, a better understanding of the sources of INPs that impact orographic clouds is important for assessing water availability in California. This study presents a multi-site, multi-year analysis of single-particle insoluble residues in precipitation samples that likely influenced cloud ice and precipitation formation above Yosemite National Park. Dust and biological particles represented the dominant fraction of the residues (64% on average). Cloud glaciation, determined using satellite observations, not only depended on high cloud tops (>5.9 km) and low temperatures (<−23 °C), but also on the presence of what were likely dust and biological INPs. The greatest prevalence of ice-phase clouds occurred in conjunction with biologically-rich residues and mineral dust rich in calcium, followed by iron and aluminosilicates. Dust and biological particles are known to be efficient INPs, thus these residues likely influenced ice formation in clouds above the sites and subsequent precipitation quantities reaching the surface during events with similar meteorology. The goal of this study is to use precipitation chemistry information to gain a better understanding of the potential sources of INPs in the south-central Sierra Nevada, where cloud-aerosol-precipitation interactions are poorly understood and where mixed-phase orographic clouds represent a key element in the generation of precipitation and thus the water supply in California.

© 2016 Elsevier Ltd. All rights reserved.

1. Introduction

Mixed-phase clouds, such as those formed orographically, possess combinations of ice crystals and supercooled droplets. These types of clouds are important for precipitation processes,

* Corresponding author. NOAA Earth System Research Laboratory, 325 Broadway, R/PSD2, Boulder, CO, 80305, USA.

E-mail address: jessie.creamean@noaa.gov (J.M. Creamean).

such as the seeder-feeder mechanism (Barros and Kuligowski, 1998; Choulaton and Perry, 1986; Purdy et al., 2005). Deep and cold orographic cloud systems have been shown to produce precipitation in the ice phase (Coplen et al., 2008), meaning an initial abundance of cloud ice crystals. However, layers of supercooled liquid water have been observed to persist in clouds down to $-40\text{ }^{\circ}\text{C}$ (Korolev et al., 2003). For instance, previous work has shown that cold, deep convective clouds can contain liquid water droplets, even down to $-37.5\text{ }^{\circ}\text{C}$ and particularly at cloud top (Rauber and Tokay, 1991; Rosenfeld and Woodley, 2000). In order for ice to be present at temperatures above roughly $-36\text{ }^{\circ}\text{C}$, aerosol particles that serve as ice nucleating particles (INPs) are required (DeMott et al., 2010; Murray et al., 2012; Vali et al., 2015). Mineral dust aerosols have been shown to serve as INPs in model simulations, laboratory measurements, and field studies (Atkinson et al., 2013; DeMott et al., 2003; Knopf and Koop, 2006). However, dust INPs efficiency can be contingent upon the specific mineralogy (Hoose et al., 2008) or the extent to which it has been atmospherically processed (Cziczo et al., 2009; Kulkarni et al., 2014; Sullivan et al., 2010a, 2010b). Biological material, either alone as bacteria, fungi, or pollen, or that associated with soil dust, has been shown to serve as the most efficient INPs, forming cloud ice at temperatures as high as $-1\text{ }^{\circ}\text{C}$ (Christner et al., 2008; Conen et al., 2011; Morris et al., 2004; O'Sullivan et al., 2014; Pratt et al., 2009). The presence of INPs in mixed-phase clouds has implications not only for ice formation, but also for precipitation originating from these clouds via secondary ice formation and aggregation (Bergeron, 1935; Hosler et al., 1957). However, conflicting results exist regarding the global impact of different sources of INPs on cloud formation (DeMott et al., 2010; Hoose et al., 2008, 2010a), and thus subsequent precipitation formation.

In regions with orographically-enhanced cloud formation such as California's Sierra Nevada (Pandey et al., 1999), ice nucleation is thought to occur (Meyers et al., 1992) and INPs have been shown to become incorporated within the tops of these clouds (Creamean et al., 2013). Thus, precipitation supplying water to the Sierra Nevada and the remainder of California is influenced by both mineral dust and biological INPs, which often originate from long-range transported sources (Ault et al., 2011; Creamean et al., 2013, 2015; VanCuren, 2006). Intensive, multi-agency field campaigns such as CalWater 1 (2009–2011) and CalWater 2 (2015–present) have focused on understanding the role of aerosols during winter storms driven by atmospheric rivers (ARs; narrow, meridional bands of water vapor that extend from the tropics) in California, whereby high altitude *trans*-Pacific aerosol plumes intersect low level plumes of moisture from ARs as they are orographically lifted along the Sierra Barrier (Creamean et al., 2013; Ralph et al., 2015). These winter storms increase snowpack in the Sierra Nevada, which then provides a steady source of water to regional reservoirs during the spring melt season. However, recent impacts from severely reduced snowfall, and subsequent drought in California, provide increased motivation to understand the factors that influence winter precipitation and, thus, improve forecast models and aid the preparation for future cases of severe drought (or flooding). Therefore, observational studies are needed to improve simulations of INPs not only on a global scale, but also on a regional basis as INPs impacts on precipitation can have significant implications for maintenance of water supplies in marginally dry regions.

Although most previous studies concentrated on the northern and central Sierra Nevada, recent studies have shown that mineral dust is frequently transported to the southern Sierra Nevada as well (Axson et al., 2015; Creamean et al., 2014b; Vicars and Sickman, 2011), demonstrating the broad scale implications of long-range transported aerosols on the water budget in California. This is particularly important for the higher elevation southern Sierra

Nevada Mountains, which produce deeper ascent with higher cloud tops that should be more capable of extending into the dust layers transported at high-altitudes and impact precipitation formation processes more regularly. The work presented herein focuses on understanding the types of aerosols that affected precipitation at three separate sites in Yosemite National Park in the southern domain of the Sierra Nevada. Previous work has used precipitation chemistry to evaluate the effects of aerosol sources on cloud glaciation in other regions around the globe (Zipori et al., 2015). We build upon previous measurements of insoluble residues found in precipitation samples collected in the northern Sierra Nevada (e.g., Creamean et al., 2015), adding measurements from multiple, high-elevation sites during two subsequent winter seasons (2011 and 2012). We present a more detailed investigation of the chemistry of insoluble precipitation residues as compared to one location in the northern Sierra Nevada in our previous work, with particular focus on dust and biological residues that serve as INPs. Our objectives are to: 1) investigate the detailed chemical composition of precipitation residues in Yosemite and compare with cloud and precipitation properties in the context of storm meteorology, 2) demonstrate the applicability of the methodology to a variety of locations (i.e., not just the site in the northern Sierra Nevada), and 3) provide a spatial and temporal evaluation of residues and their potential influences on cloud ice formation, which subsequently impacts precipitation reaching the surface through mechanisms such as the orographic seeder-feeder process. Results such as those presented here will be useful for assessing the factors that impact water resources in California.

2. Methods

2.1. Sample collection sites

Precipitation samples were collected at three locations in Yosemite National Park from 14 Feb – 16 Mar 2011 and 12 Feb – 29 Mar 2012. The sites, shown in Fig. 1, include Crane Flat (CFT; 1900 m above mean sea level (MSL); 38.11°N , 119.84°W), Badger Pass (BPS; 2200 m MSL; 37.67°N , 119.65°W), and Tuolumne Meadows (TMD; 2200 m MSL; 37.67°N , 119.65°W).

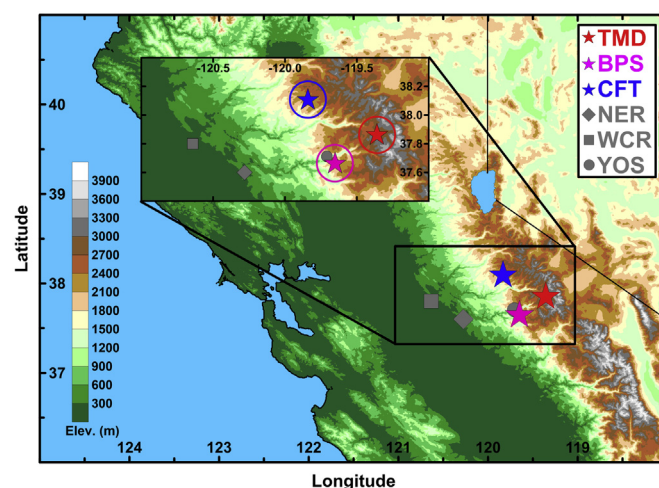


Fig. 1. Map of precipitation collection and meteorological observational sites within the vicinity of Yosemite National Park. Precipitation collection sites include Tuolumne Meadows (TMD), Badger Pass (BPS), and Crane Flat (CFT). Precipitation rate data were acquired from rain gages at the Yosemite Turtleback Dome (YOS) and New Excelsior Dam (NER) sites. Precipitation process estimated by radar was also determined from profiling radar at NER. Integrated water vapor (IWV) data were acquired from Wild Creek (WCR). Inset shows zoomed in surrounding topography, including domains surrounding each site for GOES observations, denoted by the circles.

2600 m MSL; 37.87°N, 119.36°W; 2011 only). Collection start and end times for each sample are provided in Table 1. Samples were collected in 5-gallon polytetrafluoroethylene (PTFE)-lined bags, sealed with a PTFE clip after collection, then frozen and stored up to 43 weeks until analysis. Teflon® PTFE-coated collection receptacles have been widely used for precipitation collection and storage with little to no particulate loss (Ferrari et al., 2000; Herbert et al., 2004; Sekaly et al., 1999; Stossel and Prange, 1985).

2.2. Precipitation residue chemical composition

The chemical composition of the insoluble precipitation residue particles between roughly 0.2 and 3.0 μm in vacuum aerodynamic diameter (D_{va}) was determined using aerosol time-of-flight mass spectrometry (ATOFMS) as described previously (Ault et al., 2011; Creamean et al., 2015, 2014a, 2013; Gard et al., 1997). Briefly, approximately 100–200 mL of the precipitation samples were atomized using a Collison nebulizer; re-aerosolized residues from the atomized precipitation were dried using two silica gel driers before entering the nozzle inlet of the ATOFMS. Individual residues were collimated through sequential vacuum chambers and then passed through two continuous wave scattering laser beams (532 nm) at a set distance apart, where the size of each residue was determined. The residues then moved through a third pulsed Nd:YAG laser (266 nm) where residue particles were desorbed and ionized, simultaneously creating both positive and negative ions that were then analyzed in the dual-polarity mass spectrometer. This re-aerosolization method can produce soluble and insoluble particles, agglomerates of different particle types, and insoluble particles coated with soluble species (Creamean et al., 2014a; Holecek et al., 2007a). Further, sizing of the residues is not discussed due to the modifications the residues potentially experience during re-aerosolization and drying, in addition to production of extraneous water droplets (Axson et al., 2015). Despite the caveats, this method has provided useful information on the composition of

precipitation particles as demonstrated by our previous work. Further, laboratory control experiments on known standards including dust, leaf litter, and salt corroborate the residue classifications discussed herein and validate our methods (Creamean et al., 2014a).

Single particle mass spectra from each sample were imported into YAADA (Allen, 2004), a software toolkit for Matlab (The Mathworks, Inc.). An adaptive resonance theory based clustering algorithm (ART-2a) (Song et al., 1999) was then used to group single particle mass spectra into clusters based upon similarities in the presence and intensity of ion peaks. The ART-2a identified clusters account for >90% of the total residues analyzed by ATOFMS. Previous work from Creamean et al. (2014a; 2013) and Ault et al. (2011) involved manual classification of insoluble precipitation residues. Manual classification was compared with ART-2a and both methods produced very similar results (6–10% difference between manual classification and ART-2a) (Creamean et al., 2015). The standard error (SE) was calculated for the relative amount of each different classification type of residue using the following equation, where x = the fraction of each residue type.

$$SE = \sqrt{\frac{x(1-x)}{100}}$$

2.3. Cloud microphysical properties

Data from the Geostationary Operational Environmental Satellites, GOES-11 (2011) and GOES-15 (2012) were used to define cloud phase (i.e., ice versus liquid), cloud top height, and effective cloud temperature over each of the Yosemite sites. The GOES satellite is centered at 135°W over the eastern Pacific Ocean. Cloud properties were retrieved hourly for each of the sampling days in 2011 and 2012. The five-channel GOES imager includes a visible channel (~0.65 μm) and four infrared channels, including one with a central

Table 1
Collection start and end times and the percentages of each residue type per sample collected at the three sites in Yosemite National Park during 2011 and 2012.

Year	Site	Start time (PST)	End time (PST)	Dust	Biological	Pollution	Biomass burning	Other
2011	TMD	16-Feb 14:00	17-Feb 08:00	93.56%	1.07%	1.83%	0.97%	2.58%
		17-Feb 08:00	18-Feb 08:00	84.66%	0.20%	13.29%	1.84%	0.00%
		18-Feb 08:00	19-Feb 08:00	91.19%	0.10%	4.66%	3.85%	0.20%
		24-Feb 08:00	25-Feb 08:05	85.43%	0.35%	3.25%	9.88%	1.10%
		06-Mar 08:00	07-Mar 08:05	91.04%	1.21%	5.04%	2.72%	0.00%
		15-Mar 08:00	16-Mar 16:00	66.88%	4.10%	19.89%	9.13%	0.00%
2011	BPS	14-Feb 13:45	17-Feb 11:45	77.96%	10.19%	8.32%	3.53%	0.00%
		17-Feb 11:50	22-Feb 13:10	53.70%	21.48%	20.62%	4.07%	0.12%
		24-Feb 08:00 ^a	26-Feb 11:15	76.49%	15.22%	4.43%	2.89%	0.96%
2012	BPS	06-Mar 11:00	07-Mar 10:40	84.18%	6.12%	1.05%	8.44%	0.21%
		27-Feb 08:00 ^a	28-Feb 08:00 ^a	95.09%	1.76%	1.76%	1.39%	0.00%
		28-Feb 08:00 ^a	01-Mar 08:00 ^a	89.20%	4.40%	4.00%	2.40%	0.00%
		06-Mar 04:00	06-Mar 16:40	74.96%	5.30%	16.02%	3.73%	0.00%
		13-Mar 16:00	14-Mar 12:40	86.04%	0.16%	0.81%	13.00%	0.00%
		17-Mar 13:30	18-Mar 12:30	89.97%	0.81%	6.23%	2.98%	0.00%
2011	CFT	25-Mar 12:00	26-Mar 10:30	87.61%	0.23%	0.23%	11.70%	0.23%
		14-Feb 16:15	17-Feb 13:55	46.70%	41.06%	9.10%	2.60%	0.54%
		17-Feb 16:15	22-Feb 14:40	40.90%	39.89%	15.47%	3.50%	0.23%
		24-Feb 16:10	28-Feb 07:45	55.81%	26.55%	9.72%	7.41%	0.50%
		02-Mar 07:00	04-Mar 12:30	76.06%	3.04%	17.04%	3.85%	0.00%
		12-Feb 16:05	14-Feb 08:40	88.17%	5.66%	3.60%	2.57%	0.00%
2012	CFT	14-Feb 16:00 ^a	15-Feb 16:00 ^a	75.48%	4.52%	17.85%	2.15%	0.00%
		27-Feb 08:00 ^a	28-Feb 08:00 ^a	96.61%	0.78%	0.52%	2.08%	0.00%
		28-Feb 08:00	02-Mar 08:00	86.55%	7.47%	4.08%	1.90%	0.00%
		06-Mar 08:00 ^a	07-Mar 08:00 ^a	74.69%	2.66%	20.63%	2.03%	0.00%
		17-Mar 09:30	19-Mar 06:45	65.10%	26.85%	3.02%	5.03%	0.00%
		25-Mar 10:00	26-Mar 13:45	92.07%	2.33%	4.70%	0.64%	0.26%
		28-Mar 05:30	29-Mar 08:00 ^a	91.93%	0.52%	1.30%	6.25%	0.00%

^a Exact sample times were not acquired: these are estimated times.

wavelength at 3.9 μm used to discriminate water from ice clouds. The nominal 4-km pixel GOES data were analyzed each hour for a domain surrounding each of the three sites using the methods described by Minnis et al. (2011) and applied as discussed by Minnis et al. (2008). Data from all parallax-corrected pixels within a 10-km radius of each of the three Yosemite sites (Fig. 1) were averaged to produce a variety of parameters including mean ice cloud percentage, cloud top height (Z_{top}), and effective cloud temperature (T_{eff}). The percent of ice cloud is defined as the number of cloudy pixels classified as ice divided by the total number of cloudy pixels and T_{eff} is defined as the upward radiating temperature of the cloud. Note that for percent of ice cloud, previous works by Creamean et al. (2015, 2013) have used the term “percentage of cloud ice” although these parameters are estimated using the same methods. “Ice clouds” are clouds identified as composed of ice crystals and “cloud ice” refers specifically to ice in the cloud, e.g., INPs are necessary to form “cloud ice” (cloud already exists); we identified 30% of the pixels as being “ice cloud”.

The GOES cloud phase corresponds to the water phase at the top of the cloud. It is not possible to determine the phase of the water below cloud top. Mixed phase clouds will be classified as either all ice or all liquid depending on the dominant phase at cloud top. Initial comparisons of the GOES-retrieved cloud phase with that determined from LiDAR measurements taken from the Cloud-Aerosol LiDAR and Infrared Pathfinder Satellite Observations platform (CALIPSO; Hu et al., 2009) for thick single-layer clouds show agreement of 96–99% for T_{eff} outside the supercooled cloud range of 0 to -40 °C. During the day, 87% agreement was found for T_{eff} between 0 and -20 °C that increases to 99% at -30 °C. At night, the phases are the same for 97%, 76%, and 95% of the matches for T_{eff} ranging from 0 to -10 °C, -10 °C to -30 °C, and -30 to -40 °C, respectively (Yost, 2015). Uncertainties were found to be greater over snow for non-opaque clouds. Opaque clouds are those having optical depths >3 . Most precipitating clouds in this study are opaque by that definition and, therefore, the phase selection should not be compromised by snow on the surface. For opaque clouds, T_{eff} should be accurate to within 1 K because the only correction applied is for atmospheric attenuation above the cloud. On average over the globe, the opaque physical cloud top heights retrieved with the applied algorithms are 0.02 ± 0.91 km greater and 0.61 ± 1.82 km less than the liquid and ice cloud heights, respectively, determined from CALIPSO measurements over land (Sun-Mack et al., 2014). Error bars for Z_{top} and T_{eff} in the analyses below represent the standard deviation, while error bars for % ice cloud represent the 95% confidence interval. Confidence interval is used for % ice cloud only because the values are highly variable during sample time periods due to the dynamics associated with cloud ice formation (i.e., rapid formation and loss, spatial variability, etc.) as compared to changes in cloud depth and temperature.

2.4. Meteorological characterization of events

Meteorological data were acquired from observations at multiple sites shown in Fig. 1 located in or surrounding Yosemite National Park. Although residues and cloud properties were acquired for each of the sample collection sites in Yosemite, meteorological observations were not available directly at these sites and, thus, are generalized for all of Yosemite during each event (i.e., storm) using data from the nearest observational stations. Surface meteorological measurements including hourly precipitation rate in Yosemite were acquired from the U.S. Environmental Protection Agency's (EPA) Clean Air Status and Trends Network (CASTNET; <http://www2.epa.gov/castnet>) Turtleback Dome site (YOS; 1605 m MSL; 37.71°N, 119.71°W). CASTNET precipitation totals were calculated

per day and presented herein. Precipitation rates (2-min) were also acquired from the New Exchequer Dam site (NER; 259 m MSL; 37.60°N, 120.28°W) as a part of the Hydrometeorological Automated Data System (HADS) network. NER is upwind of YOS, providing an optimal coupling of locations to evaluate orographic precipitation effects. Additionally, NER is the NOAA Hydrometeorological Testbed Network (NOAA HMT) site closest to the precipitation sample collection sites that has S-band frequency-modulated, continuous wave profiling radar (a.k.a. snow-level radar) measurements. The NOAA HMT snow-level radar (White et al., 2000) is a vertically pointing bistatic radar operating at 2835 MHz. The radar provides vertical profiles of radar reflectivity and Doppler vertical velocity (DVV) with 40-m vertical resolution from 20 m above the surface to 10 km every 37 s. In precipitation, the radar reflectivity is dominated by backscatter from hydrometeors, and thus the DVV provides a reflectivity-weighted estimate of the hydrometeor fall velocity. Several investigators (e.g., Kingsmill et al., 2006; Martner et al., 2008; Matrosov et al., 2014; Neiman et al., 2005; White et al., 2003, 2015) have used measurements from the snow-level radars and other NOAA HMT vertically pointing S-band pulsed precipitation profiling radars to investigate the microphysical properties of orographic precipitation. In particular, these studies have used a method called rainfall process partitioning to distinguish between stratiform precipitation with evidence of a melting layer radar brightband (referred to as brightband or BB rain) and a much shallower warm rain process that has a much smaller contribution from ice and does not exhibit a radar brightband (referred to as non-brightband or NBB rain). The latter is important because of its shallow nature, which often makes NBB rain difficult or impossible to detect with operational scanning Doppler radars (i.e., NOAA's WSR-88D network). Deeper clouds associated with stratiform precipitation (BB rain) may allow long-range transported aerosols to be imbedded within the clouds.

The accumulation and percentages of each precipitation process type (BB rain, NBB rain, and snow) were estimated using the rainfall process-partitioning algorithm developed by White et al. (2003), which was applied to the snow-level radar profiles obtained at NER. As in previous rainfall process partitioning studies, analysis was performed on all 30-min data periods when the precipitation rate exceeded ~ 1 mm h^{-1} . Brightband and echo top heights (km AGL) were also estimated using the snow-level radar data using methods employed by Neiman et al. (2005) and Martner et al. (2008). Echo top heights correspond to the maximum altitude where cloud hydrometeors are detected by the snow-level radar and, therefore, may not necessarily correspond to Z_{top} measured by GOES.

To further evaluate event characteristics, we investigated the amount of water vapor in the atmosphere near Yosemite and determined if each event had precipitation that developed from an AR. Integrated water vapor (IWV) provides a column measurement of water vapor. These data were acquired from a Global Positioning System receiver (GPS-Met) at the UNAVCO Wild Creek site (WCR; 114 m MSL; 37.60°N, 120.28°W) (White et al., 2013). The occurrence of an AR was determined by evaluating twice-daily composite Special Sensor Microwave Imager (SSM/I) satellite images of IWV. A 2-cm threshold for both the satellite images and the GPS-Met station was used to determine if an AR was present (Ralph et al., 2004).

Statistics for each event are provided in Table 2. Events were determined based on precipitation accumulation >0 mm at the YOS site. Precipitation totals were calculated from the start to the end of each event. Total quantities of precipitation that fell as the different process types (i.e., BB rain, NBB rain, convective rain, and snow) and averages/ranges of bright band and echo top heights are provided from the snow-level radar at NER. Averages/ranges of IWV at WCR were calculated for each event as well. Each event was also characterized as having or not having AR conditions.

Table 2

Precipitation and synoptic statistics during events where precipitation sample collection occurred at Yosemite National Park. Storm total precipitation (total quantity of per storm based on precipitation rates) were acquired from NER and YOS. Precipitation process types at the NER site include brightband (BB) rain, non-brightband (NBB) rain, convective (Conv) rain, and snow and were averaged per event. Averages and ranges for bright band and echo top heights (both in km AGL) were determined from the snow-level radar at NER. Integrated water vapor (IWV) measurements were acquired from the WCR site; averages and ranges are provided per event. Events with ARs were determined by the 2-cm threshold for both regional SSM/I satellite imagery and the GPS-Met system at WCR (Y = AR present, N = no AR). The end dates provided are inclusive in the event time period.

Year	Event	Start date (PST)	End date (PST)	Storm total NER (mm)	Storm total YOS (mm)	BB (mm)	NBB (mm)	Conv (mm)	Snow ^a (mm)	Bright band ^b (km)	Range bright band (km)	Echo top (km)	Range echo top (km)	IWV (cm)	Range IWV (cm)	AR
2011	1	16-Feb	21-Feb	78.2	108.6	72.2	3.0	1.0	2.0	1.3	1.1–2.9	4.3	0.5–6.0	1.3	0.7–1.9	Y
	2	25-Feb	27-Feb	11.8	28.2	10.8	1.0			1.4	1.2–1.6	3.6	2.4–4.4	1.0	0.5–1.7	Y
	3	02-Mar	04-Mar	3.0	18.3	3.0				1.2	1.2–1.2	3.7	3.6–3.8	1.6	1.0–2.2	Y
	4	06-Mar	08-Mar	11.2	34.0	9.3	1.9			1.2	1.1–1.4	3.9	1.9–5.1	1.8	1.0–2.5	Y
	5	14-Mar	17-Mar	14.2	43.1	8.1	6.1			1.4	1.2–2.0	3.6	2.7–4.7	2.1	0.6–3.1	Y
2012	6	12-Feb	16-Feb	54.1	25.8	54.1				1.1	0.7–1.3	3.7	2.2–5.0	1.2	0.5–2.1	N
	7	27-Feb	02-Mar	33.5	19.3	28.4	5.1			1.0	0.4–1.2	2.6	1.2–4.0	1.3	0.9–1.8	N
	8	06-Mar	07-Mar	2.8	3.5		3.0					0.7		0.8	0.3–1.7	N
	9	13-Mar	16-Mar	5.1	7.4	5.1				1.8	1.8–1.9	3.4	3.4–3.5	2.4	1.7–2.8	Y
	10	16-Mar	19-Mar	175.5	78.6	144.3	23.4	7.9		1.0	0.0–1.9	3.6	0.5–5.8	1.6	0.6–2.6	N
	11	25-Mar	28-Mar	23.1	24.0	23.1				1.2	0.8–1.5	5.0	4.8–5.2	1.5	1.2–2.3	Y

^a Liquid equivalent.

^b Height of bright band; cells left blank if bright band not present.

3. Results and discussion

3.1. Variation in cloud properties over yosemite sites each year

Cloud macrophysical properties, such as depth and temperature, can in theory largely influence the amount of ice contained within a cloud layer, particularly in pristine clouds (Rosenfeld et al., 2008). Fig. 2 shows the cloud properties, including cloud top height (Z_{top} , indicative of cloud depth), effective cloud temperature (T_{eff}), and relative amounts of ice clouds (% ice cloud), for each of the three sites during the 2011 and 2012 sample collection. The coldest (lower T_{eff}) and some of the deepest (higher Z_{top}) clouds were observed at BPS in 2012 (average $T_{eff} = -30.3$ °C, $Z_{top} = 6.5$ km), followed by TMD in 2011 (-27.8 °C and 7.0 km, respectively), then CFT in 2012 (-27.6 °C and 6.5 km, respectively). In contrast, CFT and BPS in 2011 had the lowest (5.7 and 5.9 km, respectively) and warmest cloud tops (both at -23.0 °C). Based on these results, we might expect the percent of ice cloud to be largest (smallest) when cloud tops were higher (lower) and colder (warmer). However, TMD in 2011 had the most ice clouds on average (75%), followed by BPS in 2011 (62%), CFT in 2011 (53%), and last BPS in 2012 (51%). Ice cloud percentages were overall quite variable within each year compared to Z_{top} and T_{eff} , as demonstrated by the large range between the 10th and 90th percentiles in Fig. 2C. Generally, the highest elevation site had the most glaciated clouds on average, while the lowest elevation site had the fewest glaciated clouds during 2011 sampling. The opposite effect occurred in 2012, however, the glaciation was comparable at CFT and BPS. The amount of ice cloud was not directly dependent on cloud depth and temperature as one might expect. Creamean et al. (2014b) and Rosenfeld and Woodley (2000) found that supercooled droplets can exist in clouds due to the lack of INPs, demonstrating the importance of cloud nuclei as a factor for controlling cloud ice. Cloud temperatures within the homogeneous freezing regime (approximately < -38 °C) were observed periodically during each sampling time period, i.e., T_{eff} was less than -38 °C for 17%, 10%, 30%, 12%, and 24% of the time for TMD (2011), BPS (2011), BPS (2012), CFT (2011), and CFT (2012), respectively. Thus, homogeneous freezing potentially contributed to the relative amount of ice cloud during a fraction of the sampling time period. However, the relationships observed between the cloud properties, precipitation residue particles, and precipitation suggest INPs played a strong role in cloud and precipitation formation. Herein, we demonstrate

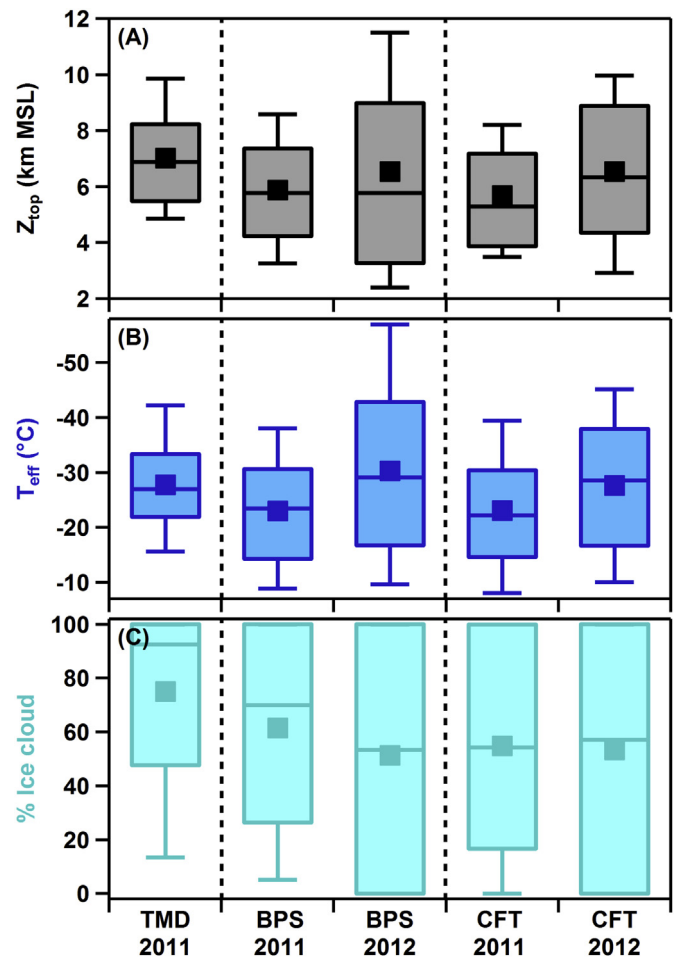


Fig. 2. Cloud properties measured by GOES averaged over each site for the 2011 and 2012 sampling time periods. Box-and-whisker plots show the data from (A) cloud top height (Z_{top}), (B) effective cloud temperature (T_{eff}), and (C) percent of ice cloud over each site, with the middle line representing the median, marker representing the average, bottom and top of the box showing the 25th and 75th percentiles, respectively, and the bottom and top whiskers showing the 10th and 90th percentiles, respectively. Note that the axis for T_{eff} is reversed so that colder (warmer) temperatures are at higher (lower) on the graph.

how precipitation residue particles that likely served as INPs in the clouds above the sites played a role in dictating cloud ice with subsequent precipitation formation, in the context of the storm meteorological conditions.

3.2. Storm meteorology during events

In order to set the stage for investigating the impacts of precipitation residue composition on cloud ice and precipitation formation, we first evaluate the meteorological conditions during each of the storms. In Yosemite, 5 separate events occurred in 2011, while 2012 had 6 separate events (see Fig. 3 and Table 2). Typically, one precipitation sample was collected at one or more of the sites during each event. Generally, all events (excluding event 3 in 2012) are characterized by comparable IWVs (1.0–2.1 cm), bright band heights (1.0–1.8 km), and echo top heights (2.6–5.0 km). Event 3 in 2012 produced the least amount of precipitation, was relatively warm (it was the only event with solely NBB rain, i.e., no bright band detected), contained the lowest IWV, and lowest echo top heights. These surface observations corroborate the ice cloud percentages and Z_{top} measured over Yosemite; event 3 from 2012 contained the lowest percent of ice cloud and Z_{top} (12% and 4.3 km, respectively, see section 3.5). The remaining events all produced cold precipitation (i.e., BB rain and/or snow) and had relatively high amounts of ice cloud and deep cloud systems (i.e., high Z_{top} and echo top heights).

Orographic precipitation in the Sierra is controlled by two atmospheric phenomena. First, the inland transport of potentially

unstable, moist, maritime air from the Pacific Ocean, which may or may not be classified as an AR, is key. Secondly, the uplift of this moisture associated with synoptic-scale ascent and/or the Sierra Barrier Jet (SBJ) is necessary to produce clouds and eventually precipitation. SBJs have been studied extensively (Kingsmill et al., 2013; Marwitz, 1983, 1987; Neiman et al., 2013; Parish, 1982; Reynolds and Dennis, 1986) and are a common occurrence during landfalling winter storms. SBJs form when stably stratified flow approaches the Sierra foothills, decelerates, and turns leftward toward the north end of the Central Valley in response to a weakened Coriolis force. Typically this happens when the atmospheric Froude number ($F_r = U/Nh$, where U is the incoming flow, N is the Brunt-Väisälä frequency, and h is the terrain height) is between 0 and 1 (Pierrehumbert and Wyman, 1985; Smolarkiewicz and Rotunno, 1990). Neiman et al. (2013) analyzed 65 SBJs that were observed in water years 2006–11 with a network of 915-MHz Doppler wind profilers (Carter et al., 1995) in Northern California. They listed several attributes of the 20 strongest SBJ cases observed with the wind profiler at Sloughouse, California, at the southern end of the Sacramento Valley and closest to the Yosemite region studied here. Three of these SBJ cases overlap with the first three storms in Table 2. For these three events, the SBJ lasted between 8 and 17 h. The altitude of the maximum wind in the SBJ varied from 621 to 1183 m. The maximum hourly wind speed in the SBJ varied between 22.4 and 24.6 $m s^{-1}$. The wind direction at the altitude of the maximum wind varied between 163.1 and 175.9°. This provides some typical attributes of strong SBJs, however it should be noted that SBJs are often weaker and shallower in the southern part of the

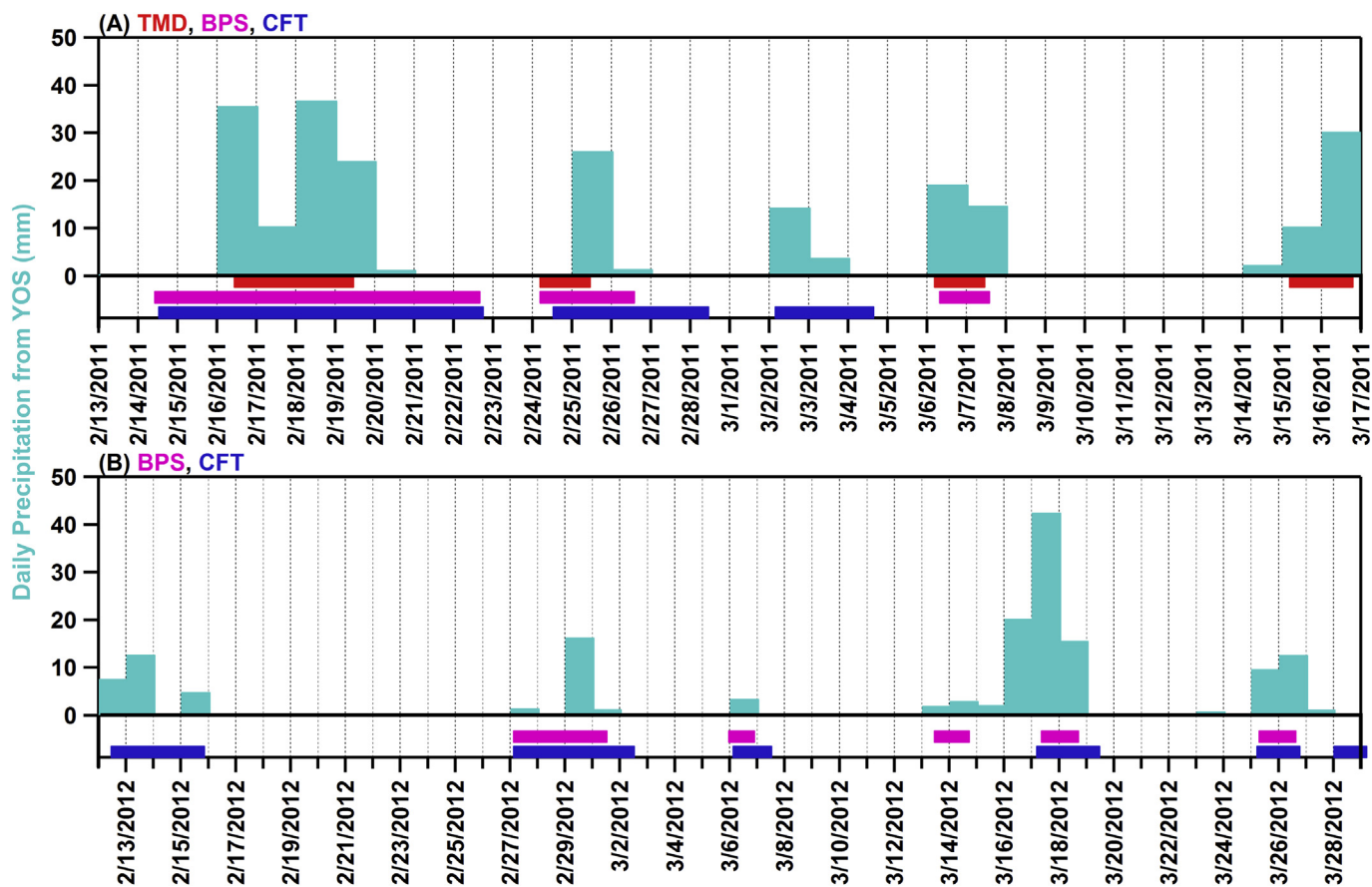


Fig. 3. Time series of daily precipitation from the YOS site during 2011 and 2012 study time periods. Colored bars at the bottom of each panel represent the time period of sample collection from each site, including TMD (red), BPS (pink), and CFT (blue). (For interpretation of the references to colour in this figure legend, the reader is referred to the web version of this article.)

Central Valley.

Potentially unstable moist maritime flow in ARs ascends over the cooler stable air in the SBJ. This was demonstrated using several type of observational datasets by Kingsmill et al. (2013) and by observations and a reanalysis dataset by Neiman et al. (2013). Both studies end with schematics that illustrate this behavior (Fig. 15 in Kingsmill et al. and Fig. 13 in Neiman et al.). This lift aids in the orographic precipitation process. Not all events studied here corresponded to ARs, even though moisture had to be available in order to produce precipitation. No correlation existed between the presence of an AR and storm total precipitation observed at YOS (see Table 2). However, a closer investigation of the relationship between hourly upslope flux of moisture and the corresponding hourly orographic precipitation response conducted by Neiman et al. (2013) indicated a robust correlation ($r = 0.93$ – 0.96) for three observing couplets in the Central Valley and Sierra foothills of northern California. It is possible that, depending on wind speed, turbulent mixing at the interface between the SBJ and the overlying moist maritime air mass may allow Central Valley aerosols to be incorporated into the clouds from below and eventually into the precipitation samples collected at the three sites in Yosemite, as will be examined in the following section.

3.3. Chemical composition of precipitation residues from each sample

Previous work has shown that insoluble residues found in precipitation samples can serve as efficient INPs and can be linked to the relative amount of ice in clouds above collection sites in the northern domain of the Sierra Nevada. It is important to note that although we derive relationships between cloud ice, precipitation properties, and precipitation residues (i.e., INPs), other factors play an important role in the location of ice formation and resulting precipitation quantity at the ground, such as wind speed, water vapor, and temperature throughout the cloud (Hobbs et al., 1973). However, we did not have vertically-resolved wind, water vapor, or temperature measurements for the current work, thus, maintain a discussion regarding potential relationships between residue type with cloud ice, and not specifics on location of ice formation. Because the focus is on ice in mixed-phase clouds and thus particles that served as INPs, we herein focus on dust and biological residues; however, Table 1 provides the relative amount of all major residue types per sample. We note that it is possible the dust and biological residues served as giant cloud condensation nuclei (CCN) in the warm region of the clouds (i.e., below the bright band), influencing cloud droplet formation (Bauer et al., 2003; Posselt and Lohmann, 2008). However, we do not assess the extent to which they served as CCN as we do not have information regarding location of nucleation within the clouds above the collection site. ATOFMS residues were classified based on previous work and had similar chemical fingerprints to those from samples collected previously in the northern Sierra Nevada (Ault et al., 2011; Creamean et al., 2014a, 2015). Briefly, the dust residues typically contained a combination of metal (i.e., sodium ($^{23}\text{Na}^+$), aluminum ($^{27}\text{Al}^+$), potassium ($^{39,41}\text{K}^+$), calcium ($^{40}\text{Ca}^+$), titanium ($^{48}\text{Ti}^+$), and iron ($^{54,56}\text{Fe}^{++}$)) and metal oxides, including aluminosilicates ($^{43}\text{AlO}^-$, $^{59}\text{AlO}_2^-$, $^{60}\text{SiO}_2^-$, $^{76}\text{SiO}_3^-$) and/or organic nitrogen and phosphorus ($^{26}\text{CN}^-$, $^{42}\text{CNO}^-$, $^{63}\text{PO}_2^-$, $^{79}\text{PO}_3^-$, $^{97}\text{PO}_4^-$) (Pratt et al., 2009; Sullivan et al., 2007). Biological residues typically comprised a combination of sodium, magnesium ($^{24}\text{Mg}^+$), potassium, calcium, and/or all of the aforementioned organic nitrogen and phosphate markers. The mass spectral signatures of “biological residues” can be differentiated from dust residues containing biological material on the basis of abundant organic and/or organic nitrogen and phosphorus ions, as well as a lack of key dust markers such as

aluminosilicates and titanium (Pratt et al., 2009). It is important to note that the purely biological residues could be a result of the re-aerosolization process, and thus they might have originally been components of the dust particles, which could be the case for purely dust residues as well (Creamean et al., 2015). Biomass burning residues varied in composition, but typically contained some combination of sodium, potassium, elemental carbon ($^{36}\text{C}_3^-$, $^{48}\text{C}_4^-$, $^{60}\text{C}_5^-$), aged organic carbon fragments ($^{27}\text{C}_2\text{H}_3^+$ / NCH^+ , $^{73}\text{CH}_3\text{CH}_2\text{CHOO}^-$), and/or polycyclic aromatic hydrocarbon markers ($^{51}\text{C}_4\text{H}_3^+$, $^{63}\text{C}_5\text{H}_3^+$, $^{77}\text{C}_6\text{H}_5^+$) (Qin and Prather, 2006; Silva et al., 1999). Pollution residues contained aged organic carbon and/or amine markers ($^{43}\text{C}_2\text{H}_3\text{O}^+$ / CHNO^+ , $^{58}\text{C}_2\text{H}_5\text{NHCH}_2^+$, $^{86}(\text{C}_2\text{H}_5)_2\text{NCH}_2^+$), with a dearth of common biomass burning markers. Both biomass burning and pollution residues also typically contained sulfate ($^{97}\text{HSO}_4^-$) and/or nitrate ($^{62}\text{NO}_3^-$).

Fig. 4 shows the percentage of dust plus biological residues (referred to as “Dust + Bio”) from each sample, in addition to the average absolute ion peak areas of common dust and biological species (i.e., ion markers) per sample. Ion peak areas can provide insight into the relative abundance of a particular species in each residue (Creamean et al., 2014a), and are discussed in more detail in the following section. During the 2011 study, the most Dust + Bio was observed in the precipitation samples collected at the highest elevations; TMD is the highest elevation site and had the greatest Dust + Bio (42–81%), while CFT is the lowest elevation site and had the least amount (26–76%). This suggests the dust and biological residues were long-range transported at higher elevations in contrast to originating from more local sources such as the California Central Valley. Creamean et al. (2016) presents a more detailed analysis of the source of residues at Yosemite collected during the 2013 winter season and concluded that the lower elevation sites, CFT and BPS, were influenced by pollution and agriculture in the Central Valley, whereas the higher elevation TMD was predominantly influenced by long-range transported mineral dust. We make the assumption here that dust and biological residues were long-range transported while pollution and biomass burning residues were predominantly local based on the plethora of previous work in this region, although future research is needed to support this (Ault et al., 2011; Creamean et al., 2015, 2014b, 2013; Jaffe et al., 2003; Uno et al., 2011; VanCuren, 2003; VanCuren and Cahill, 2002; Vicars and Sickman, 2011; Yu et al., 2012; Zhao et al., 2006). However, it is possible that the pollution and biomass burning residues could be long-range transported as well (de Gouw et al., 2004). Further, Dust + Bio residues were more abundant in the 2011 samples compared to 2012, suggesting more were transported during the 2011 sampling season. The relative amounts of Dust + Bio in the 2012 samples were highly variable, ranging from 13% to 78%, suggesting the sources were also highly variable.

3.4. Linking residue composition to cloud properties at each site each year

To provide more information regarding the types of aerosols that likely served as INPs, we present a detailed evaluation of the chemical species present in the residues. Parsing the chemical characteristics of the dust and biological residues reveals significant variations among the sites and between the sampling years as shown in Fig. 4. Fig. 5 summarizes the influence from dust residues and dust ion markers per site/sampling season, while Fig. 6 quantifies the effect for biological residues and organic nitrogen and phosphate markers. As shown in Fig. 5, dust residues contained more organic nitrogen and phosphate, i.e., had higher ion peak areas of $^{26}\text{CN}^-$, $^{42}\text{CNO}^-$, and $^{79}\text{PO}_3^-$, at lower elevations, and in 2011 compared to 2012. This is consistent with the same ion markers on

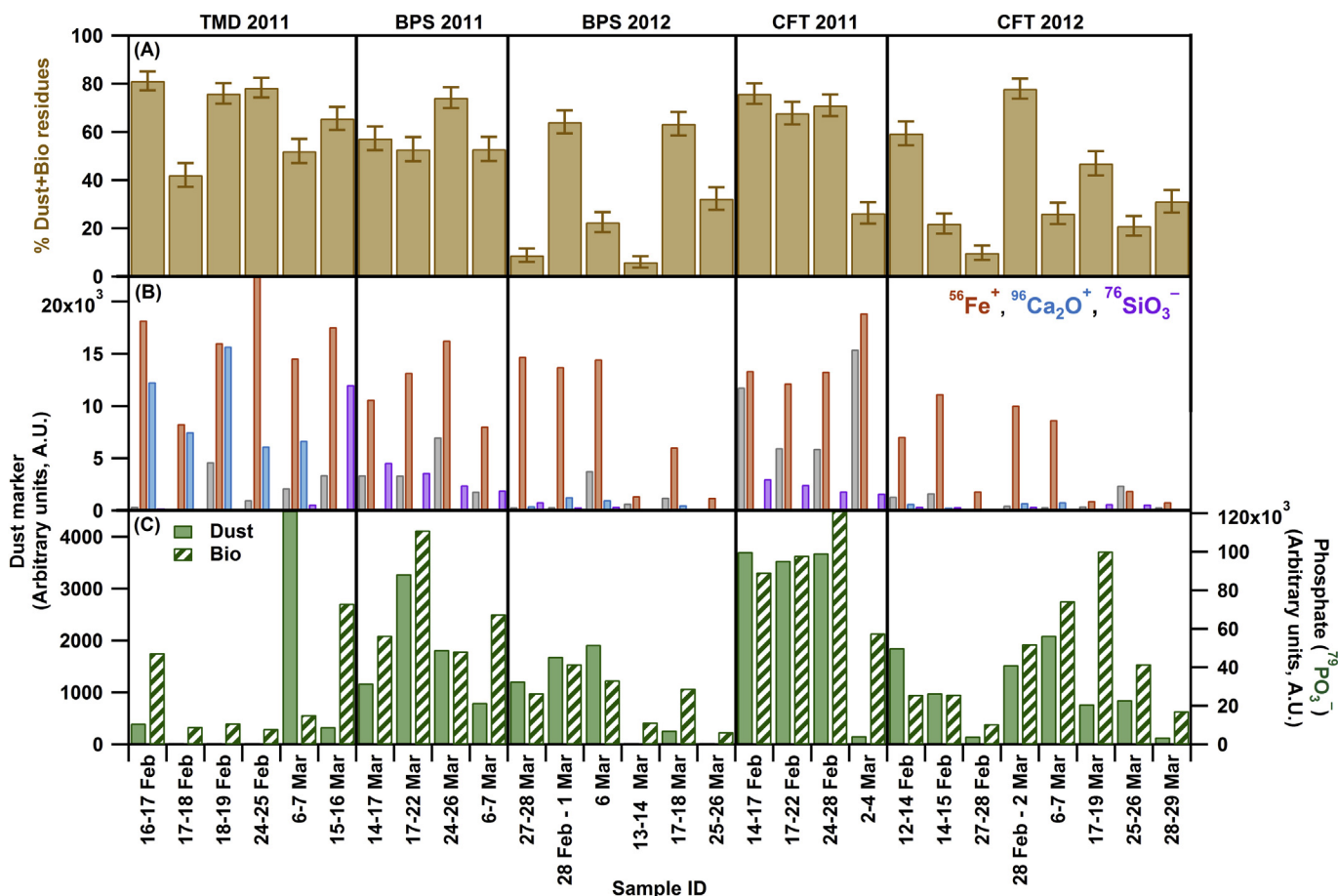


Fig. 4. Chemical composition of precipitation residues, including (A) total percentage of dust and biological residues (%Dust + Bio) from each of the precipitation sample time periods. Also shown are absolute ion peak areas from each sample, including (B) common dust ion markers ($^{56}\text{Fe}^+$, $^{96}\text{Ca}_2\text{O}^+$, $^{76}\text{SiO}_3^-$) and (C) phosphate ($^{79}\text{PO}_3^-$) found in both dust and biological residues.

the biological residues and with the average percent of biological residues per site per sampling year (see Fig. 6). The abundance of biological material in the precipitation samples at the lower elevation sites, particularly BPS and CFT, could partially explain why there was a slightly higher relative amount of ice cloud above these sites in 2011 (62% and 55% on average, respectively) compared to the same sites in 2012 (51% and 53% on average, respectively) (Conen et al., 2011; O'Sullivan et al., 2014). Further, the fact that biological particles are efficient ice nucleators at relatively high temperatures could elucidate why high relative ice cloud quantities were observed at the highest temperatures at Yosemite. Cloud temperatures were -23.0°C and -23.0°C on average at BPS and CFT in 2011 (compared to -27.8°C , -30.3°C , and -27.6°C for TMD, 2011; BPS, 2012; and CFT, 2012; respectively; see Fig. 2), and reached up to -8.9°C and -8.0°C , respectively. At these upper limits for cloud temperature, biological particles can efficiently nucleate ice, whereas mineral dust particles do not have the ability to serve as efficient INPs (Atkinson et al., 2013; Hoose et al., 2010b; Marcolli et al., 2007; Murray et al., 2012). It is important to note that the presence of good versus poor ice nucleators is also dependent on wind speed and lateral cloud extent, which influence the ice crystal population reaching the ground.

However, the average ion peak areas of organic nitrogen and phosphate in most TMD samples was not as high as those in the BPS and CFT samples, yet the TMD samples correspond to the highest relative amount of ice cloud overall. The TMD residues were calcium-rich and/or aluminosilicate-rich compared to those from

the other sites in 2011 and 2012, i.e., high ion peak areas of $^{96}\text{Ca}_2\text{O}^+$, $^{76}\text{SiO}_3^-$, and/or $^{120}\text{AlSiO}_4^-$, respectively. A unique dust subtype, calcium-rich dust classified by calcium ions ($^{40}\text{Ca}^+$, $^{56}\text{CaO}^+$, $^{57}\text{CaOH}^+$, $^{84}\text{Ca}_2^+$, $^{96}\text{Ca}_2\text{O}^+$, $^{113}(\text{CaO})_2\text{H}^+$), sulfur-related ions ($^{64}\text{SO}_2^-$, $^{80}\text{SO}_3^-$), and higher mass aluminosilicate ions ($^{119,120,121}\text{AlSiO}_4^-$, $^{136}\text{Si}_2\text{O}_5^-$, $^{137}\text{HSi}_2\text{O}_5^-$, $^{148,149,150}\text{Si}_3\text{O}_4^-$), was observed in precipitation samples collected at a site in the northern Sierra Nevada in 2011 (Creamean et al., 2013). These results suggest that different dust minerals were likely incorporated into the clouds and subsequently into the precipitation each year, chiefly at the higher elevation site. Based on the natural abundances of dust minerals (Murray et al., 2012), we hypothesize that the calcium-rich type could originate from a number of natural minerals, such as gypsum (CaSO_4), calcite (CaCO_3) aged during transportation (Dentener et al., 1996; Dunlea et al., 2009; Sullivan et al., 2007), or Ca-feldspar ($\text{CaAlSi}_3\text{O}_8$; when calcium and aluminosilicate ion markers are present within the same residue). Gypsum and Ca-feldspar have been shown to form cloud ice at temperatures up to -16°C (deposition freezing regime only) and -26°C , respectively (Atkinson et al., 2013; Zimmermann et al., 2008). Thus, the mineral dust present in the TMD samples has the potential to nucleate ice efficiently, particularly at the average cloud temperature observed above the site (-27.8°C , most within the range of -33.3°C to -27.0°C , Fig. 2). Overall, these results demonstrate that residues had variable characteristics of a mix of soil (dust with biological and other humic/organic material) and mineral dust and that different types of dust and biological residues likely induced cloud ice formation

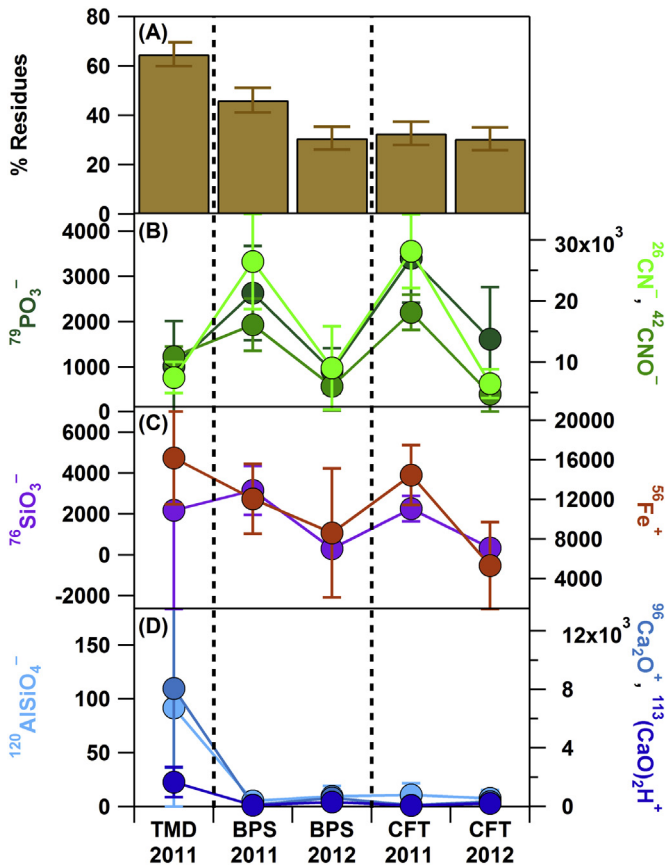


Fig. 5. Dust precipitation residue chemical characterization averaged from each site, each sampling year. (A) shows the average percent of dust residues, while (B)–(D) show specific *m/z* that are representative of dust precipitation residues, including $^{79}\text{PO}_3^-$, $^{26}\text{CN}^-$, $^{42}\text{CNO}^-$, $^{76}\text{SiO}_3^-$, $^{56}\text{Fe}^+$, $^{120}\text{AlSiO}_4^-$, $^{96}\text{Ca}_2\text{O}^+$, and $^{113}(\text{CaO})_2\text{H}^+$. Axes for ion markers are in arbitrary units (A.U.). Error bars shown represent the standard error for % residues and standard deviation for the average ion peak areas.

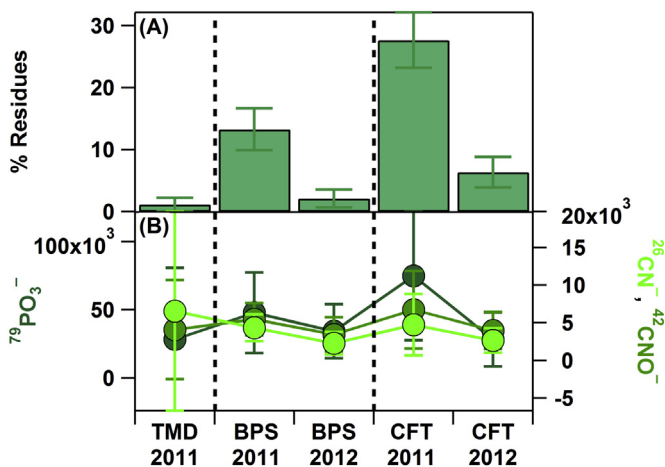


Fig. 6. Same as Fig. 5, but for the biological precipitation residue chemical characterization. Organic nitrogen and phosphate markers including $^{79}\text{PO}_3^-$, $^{26}\text{CN}^-$, and $^{42}\text{CNO}^-$ are exclusively shown. Biological residues contained little to no peak area of common dust ion markers that are shown in Fig. 5. Axes for ion markers are in arbitrary units (A.U.). Error bars shown represent the standard error for % residues and standard deviation for the average ion peak areas.

3.5. Relationships between residue, cloud, and precipitation properties during events

The abundance of dust and biological residues found in the precipitation samples potentially impacted the relative ice cloud and subsequent precipitation amounts by serving as INPs (Fig. 7). Here, we utilize averaged data from all three sites per event for comparison of the residue composition and cloud properties to event meteorology and precipitation properties during each storm because: 1) separate precipitation rate measurements were not available per site, only one total in Yosemite (YOS, Figs. 1–2) the effects of INPs on clouds and subsequent precipitation formation is a process that likely happens over larger spatial scales than over one, single location (e.g., Hong et al., 2004), and 3) one of the goals is to align with the methods of residue, cloud, and precipitation property linkages from the northern Sierra Nevada by Creamean et al. (2015, 2013) for comparison. Event 10 was eliminated from the following analysis because the average T_{eff} was $< -38^\circ\text{C}$, thus has a greater chance of influence from homogeneous nucleation.

The percentages of Dust + Bio and ice cloud are strongly correlated (Spearman's correlation coefficient (ρ) = 0.76). We employ the use of ρ to show the monotonic relationships between the residue composition and cloud properties, since the relationship between aerosols and precipitation is not a linear function of two variables and other factors such as meteorological conditions or influences prior to reaching the Sierra Nevada (i.e., orographic precipitation at the coastal mountain range) play a role (Creamean et al., 2015; Neiman et al., 2013). However, when evaluating the correlation between the Dust + Bio and ice cloud percentages for individual samples at each site (i.e., not averaging per storm), the correlation was poor (ρ = 0.40). This is likely due to the fact that glaciation is occurring upwind prior to snowfall at each site, sometimes up to 40 km upwind (Young, 1974), thus introducing time and space for secondary ice processes (i.e., splintering, riming) to occur (Meyers et al., 1992). Averaging over a larger area attempts to alleviate this issue. The percentage of ice cloud was also inversely correlated with T_{eff} (ρ = -0.88), and correlated with Z_{top} (ρ = 0.92) and storm total precipitation at YOS (ρ = 0.76), suggesting colder (warmer) and deeper (shallower) cloud systems afforded larger (smaller) quantities of precipitation. The strongest correlation of the observations shown in Fig. 7 was between the percentage of Dust + Bio and storm total precipitation (ρ = 0.90), and additionally inversely correlated with T_{eff} (ρ = -0.78). Previous modeling studies have demonstrated INP concentrations as a function of cloud temperature and ice amount, corroborating our in situ observations (Hong et al., 2004). The %Dust + Bio did not correlate strongly with the amount of ice-induced precipitation (BB rain + snow, termed IIP; ρ = 0.53), which could be due to the fact that the radar used to estimate the quantities of IIP are ~100 km upwind of the sample collection sites. Surprisingly, storm total precipitation did not correlate well with IWV (ρ = 0.08), signifying that the availability of water vapor was not a controlling factor in the amount of precipitation that fell at Yosemite. Overall, the relative amount of ice cloud was dependent not only on cloud temperature and height, but also on the presence of what were likely dust and biological INPs. These results demonstrate that the presence of ice clouds depend on a combination of availability of INPs, cloud temperature, and cloud depth (e.g., higher clouds enable intersection of transported dust and biological aerosols with regions where ice formation is efficient (Creamean et al., 2013; Meyers et al., 1992). Those parameters successively influence the process type and quantity of precipitation reaching the surface. These relationships have been observed in the northern Sierra Nevada (Creamean et al., 2013, 2015), where dust and biological particles were shown to originate from Asian, African, and Middle

above each of the Yosemite sites.

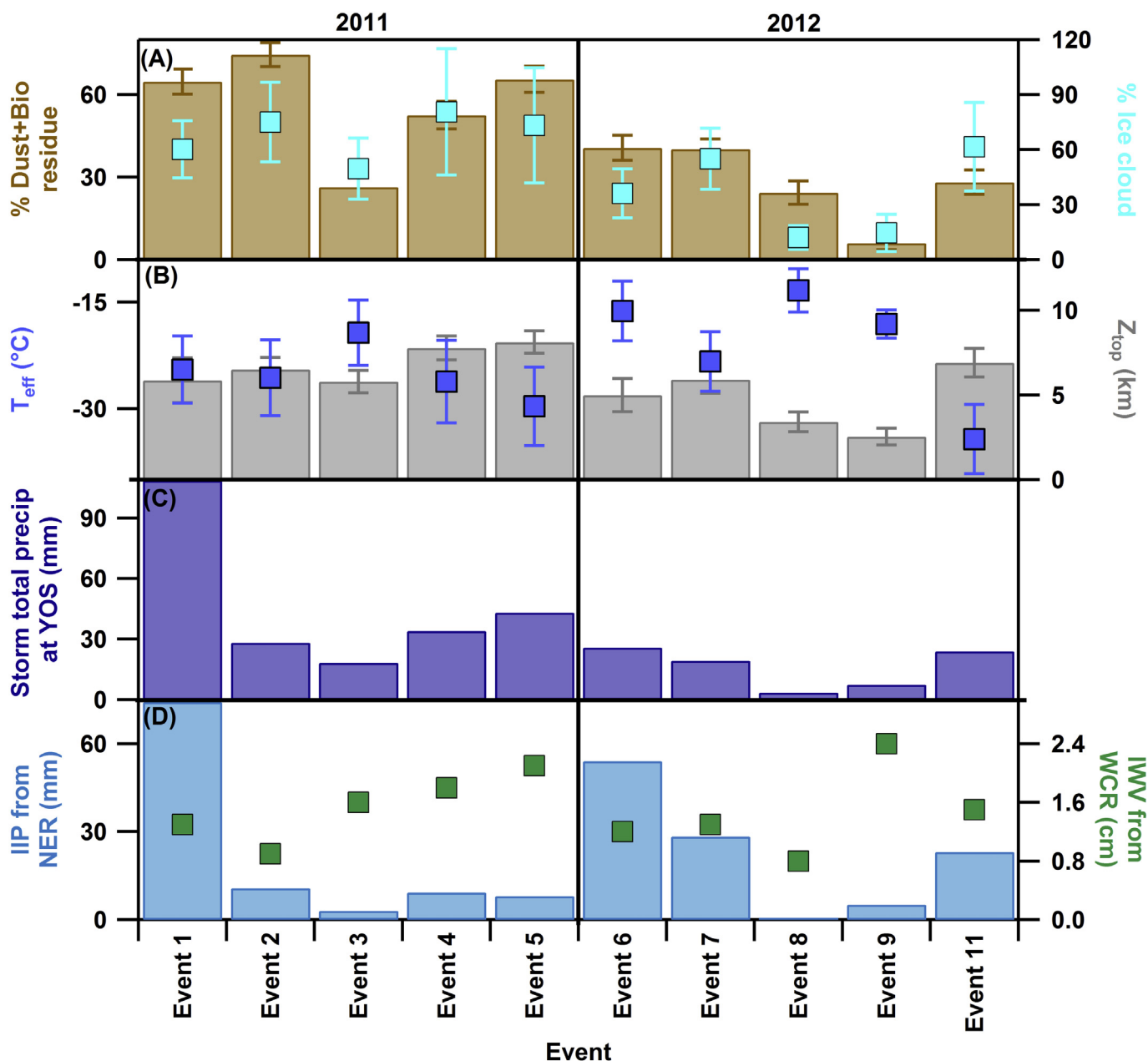


Fig. 7. Comparison between cloud properties, event meteorology, and residue composition. Observations include (A) %Dust + Bio and % ice cloud averaged from all sample collection sites combined, (B) effective cloud temperature (T_{eff}) and cloud top height (Z_{top}) measured over the Yosemite sample collection sites, (C) storm total precipitation from YOS, and (D) ice-induced precipitation (IIP) and integrated water vapor (IWV) from NER and WCR, respectively. Averages shown are per event. Error bars represent standard deviation for Z_{top} , and T_{eff} , and standard error for the %Dust + Bio, and 95% confidence interval for the % ice cloud. Event 10 is not shown because average T_{eff} was within the homogeneous nucleation regime.

Eastern deserts and influence the orographic clouds and precipitation in that region. The presence of dust and biological INPs were deduced using a combination of satellite observations, air mass trajectory modeling, in situ aircraft measurements, and ground-based precipitation collection. However, stronger correlations between residue, cloud, and precipitation properties are reported here as compared to previous studies. Further, our results demonstrate that these relationships extend farther south in the Sierra Nevada, where snowpack is potentially more valuable due to the higher terrain as compared to the northern Sierra Nevada.

Although we have previously demonstrated the utility of correlations between ice clouds and precipitation residue types, there are a number of caveats associated with the methodology that

could induce certain errors. The first is evidence that the residues were nucleated versus scavenged. This re-aerosolization method can produce agglomerates of different particle types as well as soluble coatings on insoluble residues, and therefore do not fully represent the particles that nucleated the ice in-cloud (Holecek et al., 2007b). However, agglomeration and coating processes also occur in clouds, thus, this method potentially serves as a realistic representation of aerosol-cloud interactions in nature. We did not measure ambient single-particle aerosol composition at the Yosemite sites, as in Creamean et al. (2015, 2013), to confirm that the residues were mainly absent in the ambient aerosol. Estimated ambient estimated soil concentrations from bulk aerosols samples were available through the Interagency Monitoring for Protected

Visual Environments (IMPROVE) network at YOS (<http://vista.cira.colostate.edu/improve/>); however, IMPROVE data are bulk elemental measurements and not relative single-particle observations, and are collected at very different time intervals (one 24-h sample every 3 days). Thus, they are not directly comparable to the residue composition. Aircraft measurements of cloud residues from 2011 were used to validate the presence of dust and biological particles in cloud droplets and ice crystals. These observations are presented in Fig. S4 of Creamean et al. (2013) and were measured using an aircraft version of the ATOFMS onboard the U.S. Department of Energy Gulfstream-1 (G-1) aircraft during CalWater 2011. Flight paths used for the current analysis and %Dust + Bio in cloud residues as compared to precipitation residues are shown in the Supporting Information (Figs. S1 and S2, respectively). Here, we used the flight data from the time periods when precipitation samples were collected at the Yosemite sites. The cloud residues measured on the aircraft and the precipitation residues were correlated ($\rho = 0.55$). Dust + Bio cloud residues measured on flights closest to Yosemite were within 2%–11% of the precipitation residues, supporting the assumption that the precipitation residues likely originated in cloud particles as opposed to scavenging by falling precipitation. However, the precipitation residue % Dust + Bio was higher than the cloud residues because species such as sea salt are not observed in the precipitation due to their soluble nature, thus increasing the relative contribution from dust and biological residues in the precipitation (Creamean et al., 2013, 2014a). Cloud residues are dried and analyzed individually, thus any soluble material would be observable as it effloresces as compared to the bulk precipitation samples, where the soluble material is likely present in the liquid left over after analysis (we do not aerosolize the entire volume of the precipitation samples). Overall, the in-cloud aircraft observations validate what was observed in the precipitation samples collected on the ground at Yosemite.

It is also possible that ice cloud percentage could be affected by secondary ice formation processes, such as fracturing or splintering (Hallett-Mossop). It is unlikely that Hallett-Mossop influenced the relative cloud ice because cloud temperatures were far below the -3 to -8 °C range (Hallett and Mossop, 1974). However, fracturing could play a role in the relative amount of ice cloud. Another likely source of discrepancy between the %Dust + Bio and % ice cloud is due to riming. We are unable to precisely determine if the dust and/or biological residues were from rimed droplets versus being original INPs. However, it is more likely than not that the dust and biological residues served as INPs and nucleated ice since the cloud temperatures observed were well within the range for these types of aerosols to serve as efficient INPs (Murray et al., 2012). Even considering these caveats, the aforementioned evidence supports our hypothesis that the precipitation residues likely served as INPs as opposed to being scavenged or rimed. Based on our current and previous work in the Sierra Nevada, we can still provide reasonable links between the precipitation chemistry, the aerosols that potentially nucleated cloud ice, formed precipitation, and influenced precipitation amount.

4. Summary and broader implications

We present inter-site and interannual observations of insoluble precipitation residue chemistry, cloud and precipitation properties, and surface meteorology over three locations in Yosemite National Park, USA during the 2011 and 2012 winter seasons. This study builds upon earlier research conducted using data from the northern Sierra Nevada, providing additional evidence and enabling the development of a larger spatial picture of relationships between precipitation process type and quantity, ice clouds, and

residue particles found in precipitation samples, and thus potential cloud-aerosol-precipitation interactions. Clouds were relatively cold and deep above all sites during each year, however the relative amount of ice cloud was likely dependent not only on cloud temperature and height, but also on precipitation residues that provide information on what likely served as INPs. Both calcium-rich mineral dust and biological material within the samples were present in the precipitation samples during periods of greater ice cloud coverage over the sites. We hypothesize that these residues served as the initial INPs that enabled the formation of cloud ice and influenced subsequent precipitation totals. Precipitation residues from the highest elevation site, TMD, contained dustier material rich in calcium and aluminosilicates, which we hypothesize to be from a select set of minerals capable of serving as efficient INPs. This site also had the highest relative amount of ice cloud. Precipitation residues from the lower elevation BPS and CFT sites contained more biological material, particularly in 2011, which corresponded to the next highest percentages of ice cloud. When comparing all three sites in 2011, increasing dust residues in the precipitation corresponded to increasing elevation, which is likely due to a combination of transport of potentially dust-rich air in addition to cold cloud temperatures enabling activation of the dust as INPs. When comparing events, we observed strong correlations between the relative amounts of cloud ice, residue type, and precipitation quantity, regardless of surface meteorological variations. Overall, the detailed chemical composition can provide insight into what types of residues, specifically, were potentially responsible for initiating ice formation in the clouds above the precipitation collection sites and influence the process type and quantity of precipitation reaching the ground. The fact that these results align with those from studies conducted in the northern Sierra Nevada demonstrates the utility of this method (i.e., comparing satellite-derived cloud properties, ground-based profiling of precipitation properties, and precipitation residue composition).

Generally, aerosols serving as INPs, to an extent, depend not only on clouds being high and cold enough to form cloud ice, but also on the source of the specific mineral or biological material. Further, the clouds' ability to glaciate depends heavily on the variable sources of INPs. These processes are interdependent, thus it is important to understand cloud and detailed, single-particle aerosol properties when investigating the effects of INPs on cloud ice formation. Cloud ice formation has broad implications for precipitation, in that INPs are necessary to form cloud ice, which is a key component for seeder-feeder precipitation processes, particularly in orographic, mixed-phase clouds such as those commonly present in the Sierra Nevada. INPs are one important "piece of the puzzle" in regards to developing better approximations of water supplied to the Sierra Nevada, and thus the water resources available to California. With the recent water shortage in California, it is even more important to understand the roles of INPs in cloud formation in extreme conditions such as drought due to the increased value of water during drought conditions. Although these results provide more substantial evidence that long-range transported dust and biological INPs are vital to orographic precipitation, future integration with regional forecasting and climate models is needed to evaluate how these aerosols play a role in cloud formation during periods of weak and infrequent winter storms in California.

Acknowledgments

The authors would like to acknowledge the staff at the National Park Service at Yosemite National Park for sample collection, including Katy Warner, who organized the collection protocols, Rebecca Rising, and Rob and Laura Pilewski. Ryan Spackman (NOAA/Science and Technology Corporation) and Daniel Murphy

(NOAA) provided insightful feedback. We would also like to acknowledge the California Nevada River Forecast Center (CNRFC) and DWR for providing the HADS data and CASTNET for providing the meteorological measurements at YOS. The GPS WCR site data was courtesy of the Plate Boundary Observatory (PBO) network operated by UNAVCO. Thanks to Chris Yost for providing the satellite validation results. Jessie Creamean was partially supported by the National Research Council Research Associate Program (contract number EA133F-10-CN-0187). Patrick Minnis, Rabindra Palikonda, and Doug Spangenberg were supported by the NASA Modeling, Analysis, and Prediction Program and DOE ARM Program. Data presented in the manuscript tables and figures are available by email request to the corresponding author.

Appendix A. Supplementary data

Supplementary data related to this article can be found at <http://dx.doi.org/10.1016/j.atmosenv.2016.06.016>.

References

- Allen, J.O., 2004. Quantitative Analysis of Aerosol Time-of-flight Mass Spectrometry Data Using YAADA. Arizona State University, Tempe.
- Atkinson, J.D., Murray, B.J., Woodhouse, M.T., Whale, T.F., Baustian, K.J., Carslaw, K.S., Dobbie, S., O'Sullivan, D., Malkin, T.L., 2013. The importance of feldspar for ice nucleation by mineral dust in mixed-phase clouds. *Nature* 498, 355–358.
- Ault, A.P., Williams, C.R., White, A.B., Neiman, P.J., Creamean, J.M., Gaston, C.J., Ralph, F.M., Prather, K.A., 2011. Detection of Asian dust in California orographic precipitation. *J. Geophys. Res. Atmos.* 116.
- Axson, J.L., Creamean, J.M., Bondy, A.L., Capracotta, S.S., Warner, K.Y., Ault, A.P., 2015. An in situ method for sizing insoluble residues in precipitation and other aqueous samples. *Aerosol. Sci. Tech.* 49, 24–34.
- Barros, A.P., Kuligowski, R.J., 1998. Orographic effects during a severe wintertime rainstorm in the Appalachian mountains. *Mon. Weather Rev.* 126, 2648–2672.
- Bauer, H., Giebl, H., Hitznerberger, R., Kasper-Giebl, A., Reischl, G., Zibuschka, F., Puxbaum, H., 2003. Airborne bacteria as cloud condensation nuclei. *J. Geophys. Res. Atmos.* 108.
- Bergeron, T., 1935. On the physics of cloud and precipitation. In: Dupont, Paul (Ed.), 5th Assembly of the U.G.G.I., pp. 156–178. Paris.
- Carter, D.A., Gage, K.S., Ecklund, W.L., Angevine, W.M., Johnston, P.E., Riddle, A.C., Wilson, J., Williams, C.R., 1995. Developments in UHF lower tropospheric wind profiling at NOAA aeronomy laboratory. *Radio Sci.* 30, 977–1001.
- Choulaton, T.W., Perry, S.J., 1986. A model of the orographic enhancement of snowfall by the seeder-feeder mechanism. *Q. J. Roy. Meteor. Soc.* 112, 335–345.
- Christner, B.C., Morris, C.E., Foreman, C.M., Cai, R.M., Sands, D.C., 2008. Ubiquity of biological ice nucleators in snowfall. *Science* 319, 1214–1214.
- Conen, F., Morris, C.E., Leifeld, J., Yakutin, M.V., Alewell, C., 2011. Biological residues define the ice nucleation properties of soil dust. *Atmos. Chem. Phys.* 11, 9643–9648.
- Coplen, T.B., Neiman, P.J., White, A.B., Landwehr, J.M., Ralph, F.M., Dettinger, M.D., 2008. Extreme changes in stable hydrogen isotopes and precipitation characteristics in a landfalling Pacific storm. *Geophys. Res. Lett.* 35.
- Creamean, J.M., Ault, A.P., White, A.B., Neiman, P.J., Ralph, F.M., Minnis, P., Prather, K.A., 2015. Impact of interannual variations in sources of insoluble aerosol species on orographic precipitation over California's central Sierra Nevada. *Atmos. Chem. Phys.* 15, 6535–6548.
- Creamean, J.M., Axson, J.L., Bondy, A.L., Craig, R.L., May, N.W., Shen, H., M, W., Pratt, K.A., Ault, A.P., 2016. Changes in precipitating snow chemistry with location and elevation in the California Sierra Nevada elevation. *J. Geophys. Res. Atmos.* accepted pending minor revision.
- Creamean, J.M., Lee, C., Hill, T.C., Ault, A.P., DeMott, P.J., White, A.B., Ralph, F.M., Prather, K.A., 2014a. Chemical properties of insoluble precipitation residue particles. *J. Aerosol. Sci.* 76, 13–27.
- Creamean, J.M., Spackman, J.R., Davis, S.M., White, A.B., 2014b. Climatology of long-range transported asian dust along the west coast of the United States. *J. Geophys. Res. Atmos.* 119, 12171–12185.
- Creamean, J.M., Suski, K.J., Rosenfeld, D., Cazorla, A., DeMott, P.J., Sullivan, R.C., White, A.B., Ralph, F.M., Minnis, P., Comstock, J.M., Tomlinson, J.M., Prather, K.A., 2013. Dust and biological aerosols from the sahara and asia influence precipitation in the western U.S. *Science* 339, 1572–1578.
- Cziczo, D.J., Froyd, K.D., Gallavardin, S.J., Moehler, O., Benz, S., Saathoff, H., Murphy, D.M., 2009. Deactivation of ice nuclei due to atmospherically relevant surface coatings. *Environ. Res. Lett.* 4.
- de Gouw, J.A., Cooper, O.R., Warneke, C., Hudson, P.K., Fehsenfeld, F.C., Holloway, J.S., Hubler, G., Nicks, D.K., Nowak, J.B., Parrish, D.D., Ryerson, T.B., Atlas, E.L., Donnelly, S.G., Schaubert, S.M., Stroud, V., Johnson, K., Carmichael, G.R., Streets, D.G., 2004. Chemical composition of air masses transported from Asia to the U. S. West Coast during ITCT 2K2: fossil fuel combustion versus biomass-burning signatures. *J. Geophys. Res. Atmos.* 109.
- DeMott, P.J., Prenni, A.J., Liu, X., Kreidenweis, S.M., Petters, M.D., Twohy, C.H., Richardson, M.S., Eidhammer, T., Rogers, D.C., 2010. Predicting global atmospheric ice nuclei distributions and their impacts on climate. *P Natl. Acad. Sci. U. S. A.* 107, 11217–11222.
- DeMott, P.J., Sassen, K., Poellot, M.R., Baumgardner, D., Rogers, D.C., Brooks, S.D., Prenni, A.J., Kreidenweis, S.M., 2003. African dust aerosols as atmospheric ice nuclei. *Geophys. Res. Lett.* 30.
- Dentener, F.J., Carmichael, G.R., Zhang, Y., Lelieveld, J., Crutzen, P.J., 1996. Role of mineral aerosol as a reactive surface in the global troposphere. *J. Geophys. Res. Atmos.* 101, 22869–22889.
- Dunlea, E.J., DeCarlo, P.F., Aiken, A.C., Kimmel, J.R., Peltier, R.E., Weber, R.J., Tomlinson, J., Collins, D.R., Shinzuka, Y., McNaughton, C.S., Howell, S.G., Clarke, A.D., Emmons, L.K., Apel, E.C., Pfister, G.G., van Donkelaar, A., Martin, R.V., Millet, D.B., Heald, C.L., Jimenez, J.L., 2009. Evolution of Asian aerosols during transpacific transport in INTEX-B. *Atmos. Chem. Phys.* 9, 7257–7287.
- Ferrari, C.P., Moreau, A.L., Boutron, C.F., 2000. Clean conditions for the determination of ultra-low levels of mercury in ice and snow samples. *Fresen. J. Anal. Chem.* 366, 433–437.
- Gard, E., Mayer, J.E., Morrical, B.D., Dienes, T., Fergenson, D.P., Prather, K.A., 1997. Real-time analysis of individual atmospheric aerosol particles: design and performance of a portable ATOFMS. *Anal. Chem.* 69, 4083–4091.
- Hallett, J., Mossop, S.C., 1974. Production of secondary ice particles during the riming process. *Nature* 249, 26–28.
- Herbert, B.M.J., Halsall, C.J., Fitzpatrick, L., Villa, S., Jones, K.C., Thomas, G.O., 2004. Use and validation of novel snow samplers for hydrophobic, semi-volatile organic compounds (SVOs). *Chemosphere* 56, 227–235.
- Hobbs, P.V., Easter, R.C., Fraser, A.B., 1973. A theoretical study of the flow of air and fallout of solid precipitation over mountainous terrain: Part II. Microphysics. *J. Atmos. Sci.* 30, 813–823.
- Holecek, J.C., Spencer, M.T., Prather, K.A., 2007a. Analysis of rainwater samples: comparison of single particle residues with ambient particle chemistry from the northeast Pacific and Indian oceans. *J. Geophys. Res. Atmos.* 112.
- Holecek, J.C., Spencer, M.T., Prather, K.A., 2007b. Analysis of rainwater samples: comparison of single particle residues with ambient particle chemistry from the northeast Pacific and Indian oceans. *J. Geophys. Res. Atmos.* 112.
- Hong, S.Y., Dudhia, J., Chen, S.H., 2004. A revised approach to ice microphysical processes for the bulk parameterization of clouds and precipitation. *Mon. Weather Rev.* 132, 103–120.
- Hoose, C., Kristjansson, J.E., Burrows, S.M., 2010a. How important is biological ice nucleation in clouds on a global scale? *Environ. Res. Lett.* 5.
- Hoose, C., Kristjansson, J.E., Chen, J.P., Hazra, A., 2010b. A classical-theory-based parameterization of heterogeneous ice nucleation by mineral dust, soot, and biological particles in a global climate model. *J. Atmos. Sci.* 67, 2483–2503.
- Hoose, C., Lohmann, U., Erdin, R., Tegen, I., 2008. The global influence of dust mineralogical composition on heterogeneous ice nucleation in mixed-phase clouds. *Environ. Res. Lett.* 3.
- Hosler, C.L., Jensen, D.C., Goldshlak, L., 1957. On the aggregation of ice crystals to form snow. *J. Meteorol.* 14, 415–420.
- Jaffe, D., Snow, J., Cooper, O., 2003. The 2001 Asian dust events: transport and impact on surface aerosol concentrations in the U.S. *Eos Trans. Am. Geophys. Union* 84, 501–507.
- Kingsmill, D.E., Neiman, P.J., Moore, B.J., Hughes, M., Yuter, S.E., Ralph, F.M., 2013. Kinematic and thermodynamic structures of Sierra barrier jets and overrunning atmospheric rivers during a landfalling winter storm in northern California. *Mon. Weather Rev.* 141, 2015–2036.
- Kingsmill, D.E., Neiman, P.J., Ralph, F.M., White, A.B., 2006. Synoptic and topographic variability of northern California precipitation characteristics in landfalling winter storms observed during CALJET. *Mon. Weather Rev.* 134, 2072–2094.
- Knopf, D.A., Koop, T., 2006. Heterogeneous nucleation of ice on surrogates of mineral dust. *J. Geophys. Res. Atmos.* 111.
- Korolev, A.V., Isaac, G.A., Cober, S.G., Strapp, J.W., Hallett, J., 2003. Microphysical characterization of mixed-phase clouds. *Q. J. Roy. Meteor. Soc.* 129, 39–65.
- Kulkarni, G., Sanders, C., Zhang, K., Liu, X.H., Zhao, C., 2014. Ice nucleation of bare and sulfuric acid-coated mineral dust particles and implication for cloud properties. *J. Geophys. Res. Atmos.* 119, 9993–10011.
- Marcollì, C., Gedamke, S., Peter, T., Zobrist, B., 2007. Efficiency of immersion mode ice nucleation on surrogates of mineral dust. *Atmos. Chem. Phys.* 7, 5081–5091.
- Martner, B.E., Yuter, S.E., White, A.B., Matrosov, S.Y., Kingsmill, D.E., Ralph, F.M., 2008. Raindrop size distributions and rain characteristics in California coastal rainfall for periods with and without a radar bright band. *J. Hydrometeorol.* 9, 408–425.
- Marwitz, J.D., 1983. The kinematics of orographic air-flow during Sierra storms. *J. Atmos. Sci.* 40, 1218–1227.
- Marwitz, J.D., 1987. Deep orographic storms over the Sierra-Nevada. I. Thermodynamic and kinematic structure. *J. Atmos. Sci.* 44, 159–173.
- Matrosov, S.Y., Ralph, F.M., Neiman, P.J., White, A.B., 2014. Quantitative assessment of operational weather radar rainfall estimates over California's northern sonoma county using HMT-west data. *J. Hydrometeorol.* 15, 393–410.
- Meyers, M.P., Demott, P.J., Cotton, W.R., 1992. New primary ice-nucleation parameterizations in an explicit cloud model. *J. Appl. Meteorol.* 31, 708–721.
- Minnis, P., Sun-Mack, S., Young, D.F., Heck, P.W., Garber, D.P., Chen, Y., Spangenberg, D.A., Arduini, R.F., Trepte Jr., Q.Z., W.L.S. Ayers, J.K., Gibson, S.C.,

- Miller, W.F., Chakrapani, V., Takano, Y., Liou, K.-N., Xie, Y., Yang, P., 2011. CERES Edition-2 cloud property retrievals using TRMM VIRS and Terra and Aqua MODIS data, Part I: Algorithms. *IEEE Trans. Geosci. Remote Sens.* 49 <http://dx.doi.org/10.1109/TGRS.2011.2144601>.
- Minnis, P., Trepte, Q.Z., Sun-Mack, S., Chen, Y., Doelling, D.R., Young, D.F., Spangenberg, D.A., Miller, W.F., Wielicki, B.A., Brown, R.R., Gibson, S.C., Geier, E.B., 2008. Cloud detection in nonpolar regions for CERES using TRMM VIRS and terra and aqua MODIS data. *IEEE T Geosci. Remote* 46, 3857–3884.
- Morris, C.E., Georgakopoulos, D.G., Sands, D.C., 2004. Ice nucleation active bacteria and their potential role in precipitation. *J. Phys. IV* 121, 87–103.
- Murray, B.J., O'Sullivan, D., Atkinson, J.D., Webb, M.E., 2012. Ice nucleation by particles immersed in supercooled cloud droplets. *Chem. Soc. Rev.* 41, 6519–6554.
- Neiman, P.J., Hughes, M., Moore, B.J., Ralph, F.M., Sukovich, E.M., 2013. Sierra barrier jets, atmospheric rivers, and precipitation characteristics in northern California: a composite perspective based on a network of wind profilers. *Mon. Weather Rev.* 141, 4211–4233.
- Neiman, P.J., Wick, G.A., Ralph, F.M., Martner, B.E., White, A.B., Kingsmill, D.E., 2005. Wintertime nonbrightband rain in California and Oregon during CALJET and PACJET: geographic, interannual, and synoptic variability. *Mon. Weather Rev.* 133, 1199–1223.
- O'Sullivan, D., Murray, B.J., Malkin, T.L., Whale, T.F., Umo, N.S., Atkinson, J.D., Price, H.C., Baustian, K.J., Browse, J., Webb, M.E., 2014. Ice nucleation by fertile soil dusts: relative importance of mineral and biogenic components. *Atmos. Chem. Phys.* 14, 1853–1867.
- Pandey, G.R., Cayan, D.R., Georgakakos, K.P., 1999. Precipitation structure in the Sierra Nevada of California during winter. *J. Geophys. Res. Atmos.* 104, 12019–12030.
- Parish, T.R., 1982. Barrier winds along the Sierra-Nevada mountains. *J. Appl. Meteorol.* 21, 925–930.
- Pierrehumbert, R.T., Wyman, B., 1985. Upstream effects of mesoscale mountains. *J. Atmos. Sci.* 42, 977–1003.
- Posselt, R., Lohmann, U., 2008. Influence of giant CCN on warm rain processes in the ECHAM5 GCM. *Atmos. Chem. Phys.* 8, 3769–3788.
- Pratt, K.A., DeMott, P.J., French, J.R., Wang, Z., Westphal, D.L., Heymsfield, A.J., Twohy, C.H., Prenni, A.J., Prather, K.A., 2009. In situ detection of biological particles in cloud ice-crystals. *Nat. Geosci.* 2, 397–400.
- Purdy, J.C., Austin, G.L., Seed, A.W., Cluckie, I.D., 2005. Radar evidence of orographic enhancement due to the seeder feeder mechanism. *Meteorol. Appl.* 12, 199–206.
- Qin, X.Y., Prather, K.A., 2006. Impact of biomass emissions on particle chemistry during the California regional particulate air quality study. *Int. J. Mass Spectrom.* 258, 142–150.
- Ralph, F.M., Neiman, P.J., Wick, G.A., 2004. Satellite and CALJET aircraft observations of atmospheric rivers over the eastern north pacific ocean during the winter of 1997/98. *Mon. Weather Rev.* 132, 1721–1745.
- Ralph, F.M., Prather, K.A., Cayan, D., Spackman, J.R., DeMott, P., Dettinger, M., Fairall, C., Leung, R., Rosenfeld, D., Rutledge, S., Waliser, D., White, A.B., Cordeira, J., Martin, A., Helly, J., Intrieri, J., 2015. CalWater field studies designed to quantify the roles of atmospheric rivers and aerosols in modulating U.S. West coast precipitation in a changing climate. *B Am. Meteorol. Soc.*
- Rauber, R.M., Tokay, A., 1991. An explanation for the existence of supercooled water at the top of cold clouds. *J. Atmos. Sci.* 48, 1005–1023.
- Reynolds, D.W., Dennis, A.S., 1986. A review of the Sierra cooperative pilot project. *B Am. Meteorol. Soc.* 67, 513–523.
- Rosenfeld, D., Lohmann, U., Raga, G.B., O'Dowd, C.D., Kulmala, M., Fuzzi, S., Reissell, A., Andreae, M.O., 2008. Flood or drought: how do aerosols affect precipitation? *Science* 321, 1309–1313.
- Rosenfeld, D., Woodley, W.L., 2000. Deep convective clouds with sustained supercooled liquid water down to -37.5 degrees C. *Nature* 405, 440–442.
- Sekaly, A.L.R., Chakrabarti, C.L., Back, M.H., Gregoire, D.C., Lu, J.Y., Schroeder, W.H., 1999. Stability of dissolved metals in environmental aqueous samples: rideau River surface water, rain and snow. *Anal. Chim. Acta* 402, 223–231.
- Silva, P.J., Liu, D.Y., Noble, C.A., Prather, K.A., 1999. Size and chemical characterization of individual particles resulting from biomass burning of local Southern California species. *Environ. Sci. Technol.* 33, 3068–3076.
- Smolarkiewicz, P.K., Rotunno, R., 1990. Low frequency-number flow past 3-Dimensional obstacles .2. Upwind flow reversal zone. *J. Atmos. Sci.* 47, 1498–1511.
- Song, X.H., Hopke, P.K., Fergenson, D.P., Prather, K.A., 1999. Classification of single particles analyzed by ATOFMS using an artificial neural network, ART-2A. *Anal. Chem.* 71, 860–865.
- Stossel, R.P., Prange, A., 1985. Determination of trace-elements in rainwater by total-reflection x-ray-fluorescence. *Anal. Chem.* 57, 2880–2885.
- Sullivan, R.C., Guazzotti, S.A., Sodeman, D.A., Prather, K.A., 2007. Direct observations of the atmospheric processing of Asian mineral dust. *Atmos. Chem. Phys.* 7, 1213–1236.
- Sullivan, R.C., Miñambres, L., DeMott, P.J., Prenni, A.J., Carrico, C.M., Levin, E.J.T., Kreidenweis, S.M., 2010a. Chemical processing does not always impair heterogeneous ice nucleation of mineral dust particles. *Geophys. Res. Lett.* 37.
- Sullivan, R.C., Petters, M.D., DeMott, P.J., Kreidenweis, S.M., Wex, H., Niedermeier, D., Hartmann, S., Clauss, T., Stratmann, F., Reitz, P., Schneider, J., Sierau, B., 2010b. Irreversible loss of ice nucleation active sites in mineral dust particles caused by sulphuric acid condensation. *Atmos. Chem. Phys.* 10, 11471–11487.
- Sun-Mack, S., Minnis, P., Chen, Y., Kato, S., Yi, Y.H., Gibson, S.C., Heck, P.W., Winker, D.M., 2014. Regional apparent boundary layer lapse rates determined from CALIPSO and MODIS data for cloud-height determination. *J. Appl. Meteorol. Clim.* 53, 990–1011.
- Uno, I., Eguchi, K., Yumimoto, K., Liu, Z., Hara, Y., Sugimoto, N., Shimizu, A., Takemura, T., 2011. Large Asian dust layers continuously reached North America in April 2010. *Atmos. Chem. Phys.* 11, 7333–7341.
- Vali, G., DeMott, P.J., Mohler, O., Whale, T.F., 2015. Technical Note: a proposal for ice nucleation terminology. *Atmos. Chem. Phys.* 15, 10263–10270.
- VanCuren, R.A., 2003. Asian aerosols in North America: extracting the chemical composition and mass concentration of the Asian continental aerosol plume from long-term aerosol records in the western United States. *J. Geophys. Res. Atmos.* 108.
- VanCuren, R.A., 2006. Asian aerosols in North America: extracting the chemical composition and mass concentration of the Asian continental aerosol plume from long-term aerosol records in the western United States (vol. 108, pg 4623, 2003). *J. Geophys. Res. Atmos.* 111.
- VanCuren, R.A., Cahill, T.A., 2002. Asian aerosols in North America: frequency and concentration of fine dust. *J. Geophys. Res. Atmos.* 107.
- Vicars, W.C., Sickman, J.O., 2011. Mineral dust transport to the Sierra Nevada, California: loading rates and potential source areas. *J. Geophys. Res. Biogeo.* 116.
- White, A.B., Anderson, M.L., Dettinger, M.D., Ralph, F.M., Hinojosa, A., Cayan, D.R., Hartman, R.K., Reynolds, D.W., Johnson, L.E., Schneider, T.L., Cifelli, R., Toth, Z., Gutman, S.I., King, C.W., Gehrke, F., Johnston, P.E., Walls, C., Mann, D., Gotta, D.J., Coleman, T., 2013. A twenty-first-century California observing network for monitoring extreme weather events. *J. Atmos. Ocean. Tech.* 30, 1585–1603.
- White, A.B., Jordan, J.R., Martner, B.E., Ralph, F.M., Bartram, B.W., 2000. Extending the dynamic range of an S-band radar for cloud and precipitation studies. *J. Atmos. Ocean. Tech.* 17, 1226–1234.
- White, A.B., Neiman, P.J., Creamean, J.M., Coleman, T., Ralph, F.M., Prather, K.A., 2015. The impacts of California's san Francisco bay area gap on precipitation observed in the Sierra Nevada during HMT and CalWater. *J. Hydrometeorol.* 16, 1048–1069.
- White, A.B., Neiman, P.J., Ralph, F.M., Kingsmill, D.E., Persson, P.O.G., 2003. Coastal orographic rainfall processes observed by radar during the California land-falling jets experiment. *J. Hydrometeorol.* 4, 264–282.
- Yost, C., 2015. Personal Communication.
- Young, K.C., 1974. A numerical simulation of wintertime, orographic precipitation: Part II. Comparison of natural and AgI-seeded conditions. *J. Atmos. Sci.* 31, 1749–1767.
- Yu, H.B., Remer, L.A., Chin, M., Bian, H.S., Tan, Q., Yuan, T.L., Zhang, Y., 2012. Aerosols from overseas rival domestic emissions over north America. *Science* 337, 566–569.
- Zhao, T.L., Gong, S.L., Zhang, X.Y., Blanchet, J.P., McKendry, I.G., Zhou, Z.J., 2006. A simulated climatology of Asian dust aerosol and its trans-Pacific transport. Part I: mean climate and validation. *J. Clim.* 19, 88–103.
- Zimmermann, F., Weinbruch, S., Schutz, L., Hofmann, H., Ebert, M., Kandler, K., Worringer, A., 2008. Ice nucleation properties of the most abundant mineral dust phases. *J. Geophys. Res. Atmos.* 113.
- Zipori, A., Rosenfeld, D., Tirosh, O., Teutsch, N., Erel, Y., 2015. Effects of aerosol sources and chemical compositions on cloud drop sizes and glaciation temperatures. *J. Geophys. Res. Atmos.* 120, 9653–9669.